Nanoparticles charge response from electrostatic force microscopy

A. Mottaghizadeh, P. L. Lang, L. M. Cui, J. Lesueur, J. Li, D. N. Zheng, V. Rebuttini, N. Pinna, A. Zimmers' , and H. Aubin'

Citation: Appl. Phys. Lett. **102**, 053118 (2013); doi: 10.1063/1.4790587
View online: http://dx.doi.org/10.1063/1.4790587
View Table of Contents: http://aip.scitation.org/toc/apl/102/5
Published by the American Institute of Physics

Nanoparticles charge response from electrostatic force microscopy

A. Mottaghizadeh,[1] P. L. Lang,[1,2] L. M. Cui,[1,3] J. Lesueur,[1] J. Li,[3] D. N. Zheng,[3] V. Rebuttini,[4] N. Pinna,[4,5] A. Zimmers,[1,a)] and H. Aubin[1,b)]

[1]*Laboratoire de Physique et d'Etude des Matériaux, UMR 8213, ESPCI ParisTech CNRS UPMC, 10 rue Vauquelin, 75231 Paris, France*
[2]*School of Science, Beijing University of Post and Telecommunications, Beijing 100876, China*
[3]*Beijing National Laboratory for Condensed Matter Physics & Institute of Physics, Chinese Academy of Sciences, Beijing 100190, China*
[4]*Department of Chemistry, CICECO, University of Aveiro, 3810 193 Aveiro, Portugal*
[5]*Humboldt Universität zu Berlin, Institut für Chemie, Brook Taylor Str. 2, 12489 Berlin, Germany*

(Received 5 September 2012; accepted 21 January 2013; published online 6 February 2013)

Electrostatic force microscopy (EFM) allows measurement of tiny changes in tip-sample capacitance. When nanoobjects are studied by EFM, they only contribute a very small fraction of the total capacitance between the tip and the sample. We show that the analysis of 3D maps of the EFM signal allows extracting the contribution of the nanomaterial to the total capacitance. This opens the way to applications of EFM as a measure of the dielectric coefficient of electrically insulating nanomaterials or the quantum capacitance of conducting nanomaterials. We apply this method to study the charge response of magnetite, Fe_3O_4, nanoparticles. © *2013 American Institute of Physics*. [http://dx.doi.org/10.1063/1.4790587]

As a very sensitive probe of electric field, electrostatic force microscopy (EFM) is well adapted to the study of charge response of nanosized materials. This technique has been used for discriminating insulating from metallic nanotubes,[1,2] measuring their charging capacity,[3–5] and measuring the dielectric coefficient of insulating nanoparticle (NP) and viruses.[6] EFM is also of fundamental interest as it could be used to measure the charge compressibility $\kappa = dn/d\mu$ of conducting nanomaterials. The charge compressibility is a fundamental thermodynamic property of electronic systems whose determination requires measurements of the charge response on the scale of the screening length ($\lambda \propto 1/e^2\kappa$).[7,8] For simple metals, the charge compressibility is large and is simply related to the density of states, $n \propto \mu^{3/2} \Rightarrow dn/d\mu \propto \mu^{1/2}$; in contrast, for band insulators, the charge compressibility is close to zero. In correlated electronic materials, the charge compressibility is expected to be altered by electron-electron interactions as illustrated by the transition from correlated insulators to metal[9] where it has been predicted to diverge.[10]

The major limitation of the technique is that the scanning metallic tip is capacitively coupled not only to the nanomaterial under study but also to the surrounding substrate. This hampers dramatically the extraction of quantitative information from the EFM measurements.

In this study of magnetite NPs, we show that by acquiring 3D maps of the EFM signal, it becomes possible to extract the capacitive contribution of the NP to the EFM signal, without requiring to numerical modeling of the NP-tip system. Thus, because no assumption is made on the tip or the substrate, this method makes EFM measurement more quantitative.

Magnetite has the inverse spinel structure in which the Fe^{2+} ions and half the Fe^{3+} ions are randomly distributed in the octahedral sites. The remaining Fe^{3+} ions are in the tetrahedral sites. Above the Verwey temperature ($T \sim 120$ K for bulk materials), magnetite is a semi-metal where electron transport is attributed to electron exchange between Fe^{3+} and Fe^{2+} sites. Upon decreasing the temperature, the conductivity decreases abruptly below the temperature of the Verwey transition[11] where the cations in octahedral sites order in alternating layers of Fe^{2+} and Fe^{3+} ions.

The Verwey transition is altered by size effects. For magnetite thin films, the transition is broad[12,13] and only a crossover between a high temperature metallic phase and a low temperature insulating phase is observed. In NPs, size effects are expected to broaden the Verwey transition even more. Furthermore, possible oxidation of NPs can destroy their metallic state, transforming Fe_3O_4 into its insulating sibling, the maghemite Fe_2O_3. Thus, because of disorder and oxidation, the nature of the electronic phase, metallic or insulating, is difficult to predict in magnetite NPs.

Undecanoic acid-capped Fe_3O_4 NPs of an average size of about 10 nm (Fig. 1(a)) are obtained by the reaction of iron(III) acetylacetonate in benzyl alcohol at 175 °C followed by a ligand exchange process as previously

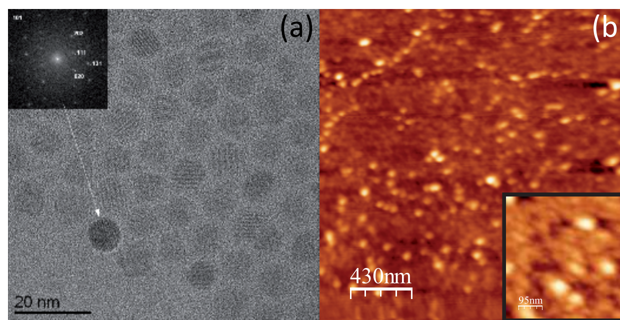

FIG. 1. Panel (a) TEM images of magnetite NPs. Inset, power spectrum of the particle indicated by the arrow. Panel (b) AFM topography image of the sample. Inset, zoom on the AFM topography image.

a)Alexandre.Zimmers@espci.fr.
b)Herve.Aubin@espci.fr.

 © 2013 American Institute of Physics

described.[14] The ligand exchange process allows the reduction of the size dispersion and to obtain a stable colloidal solution in a non-polar solvent (e.g., hexane). The NPs are highly crystalline and single crystal as demonstrated by the power spectrum in the inset of Fig. 1(a). To prepare the samples for EFM measurements, we depose a small quantity ($\sim$100 μl) of NPs onto a silicon substrate covered by a thin layer of Pd ($\sim$10 nm). To remove as much as possible of the organic ligands, the sample is baked at 300 °C in high vacuum (10^{-6} mbar).

In EFM, the electrostatic force exerted on the tip is given by

$$F = -\frac{dU_{el}}{dz} = -\frac{1}{2}\frac{\partial C}{\partial z}\Delta\phi^2, \quad (1)$$

where the electrostatic energy $U_{el} = (1/2C)\Delta\phi^2$ is a function of $\Delta\phi = \phi_{tip} - \phi_{sample} + V$, the electrochemical potential difference between the tip and the sample added to the applied voltage V, and C the total capacitance. Atomic force microscopy (AFM) and EFM measurements are carried out with a home-built variable temperature microscope installed in ultra high vacuum. The force detection is based on measurement of frequency shift f of a quartz tuning fork, which depends on the force exerted on the tip through the relation $f = -dF/dz$.[15] Typical amplitude oscillation of the tuning fork is about 5 nm. The Pt/Ir 200 nm radius tips glued onto the tuning fork were prepared by electrochemical etching. Topographic images are typically recorded with a frequency shift of f set to -4 Hz, Fig. 1(b).

To improve EFM resolution, an AC voltage ($V_{AC} \sim 500$ mV, $\omega = 30$ Hz) is applied in addition to the DC voltage ($V_{DC} = 1$ V), which gives a total applied voltage $V = V_{DC} + V_{AC}\cos(\omega t)$. This leads to a frequency shift due to electrostatic force given by

$$f(Hz) = f_{DC} + f_\omega \cos(\omega t) + f_{2\omega}\cos(2\omega t)$$
$$f_{DC} = \frac{1}{2}C''(z)\left[V_{DC}^2 + \frac{V_{AC}^2}{2}\right] \quad (2)$$
$$f_\omega = C''(z)V_{DC}V_{AC}, \quad f_{2\omega} = C''(z)V_{AC}^2,$$

where $C'' = \frac{\partial^2 C}{\partial z^2}$. The first harmonic f_ω and the second harmonic $f_{2\omega}$ are measured with a lock-in amplifier. As sketched in Fig. 2(a), the following *multipass* sequence is used. For each scan line, the height z_0 is recorded. Then, the tip is rescanned at the distance $z_{j+1} = z_0 + h_j$, where h_j is a constant offset, during which all electrostatic force components ($f_\omega, f_{2\omega}, f_{DC}$) are acquired. This sequence is repeated for 9 different height offsets h_j, where $j = 1\ldots9$. This led to the formation of a three dimensional map of the electrostatic force, which takes about 10 h to acquire.

These 3D maps are shown Fig. 3 for three temperatures, $T = 300$ K, 160 K, and 70 K. Only f_ω is shown as the signal to noise for $f_{2\omega}$ was too small in those measurements. From these maps, we can extract f_{sub} and f_{NP}, the frequency shifts measured far and above the NP, respectively.

Figure 4(d) shows f_{sub} and f_{NP} as a function of h_j, which show that both quantities decrease to large negative values as the tip approaches the surface, due to the increasing capacitance between the tip and the surface. The slope of those curves change with temperature because of changes in the sensitivity of the tuning fork. As we will see below, our extraction of the contribution of the NP to the EFM signal does not depend on sensor details such as oscillation amplitude or stiffness, which is one remarkable observation of this work.

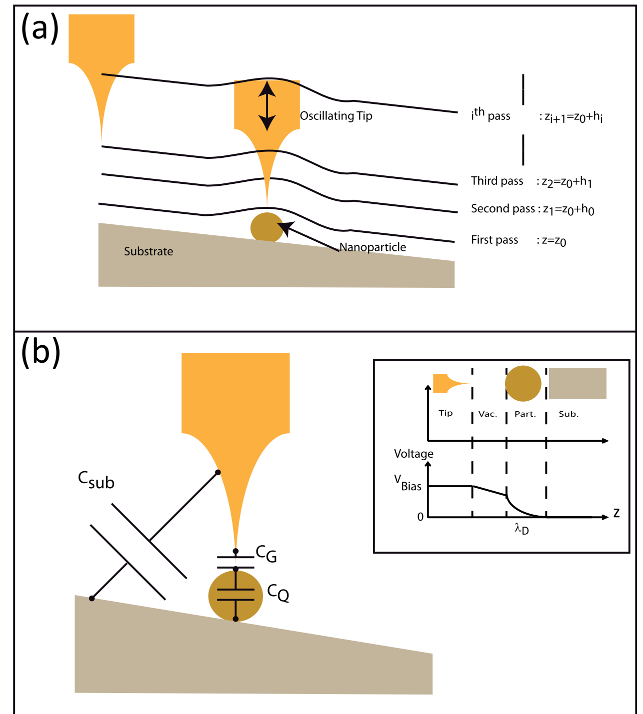

FIG. 2. Panel (a): Sketch of the *multipass* sequence used to acquire the 3D EFM map. Panel (b) main panel: Sketch of the capacitive contributions to the EFM signal. Inset: Schematic description of the evolution of the voltage from the tip to the substrate across the NP.

Figures 4(a) 4(c) show the EFM profiles $\delta f(X) = f_\omega(X) - f_{sub}$ as the NP is scanned for different heights and temperatures. In these profiles, $|f_\omega(X)|$ *decreases* as the tip scans the NP. To understand this, Fig. 2(b) provides a sketch of the different capacitive contributions to the EFM signal, which are C_{sub} the capacitance between the tip and the metallic substrate and C_{NP} the capacitance between the tip and the NP. C_{NP} includes the charge response from the NP material itself. For insulating NPs, C_{NP} depends on the dielectric coefficient ϵ of the NP through the relation $C_{NP} = \epsilon C_G$, where C_G is the geometric capacitance. For metallic NPs, $C_{NP} = C_G C_Q/(C_G + C_Q)$, where C_Q is the quantum capacitance, which is related to the electronic compressibility of the NP.[7,8]

Far (in the XY plane) from the NP, the tip/sample capacitance can simply be written as $C = C_{sub}(z = z_0 + h_j)$. Above the NP as $C = C_{NP} + C_{sub}(z = z_0 + h_j + D)$, where D is the NP diameter measured in the topography image. As the tip scans the NP in the X direction (moves above the NP), the relative change in the capacitance δC can be written as

$$\frac{\delta C}{C_{sub}} = \frac{1}{C_{sub}}\left[\frac{\partial C_{sub}}{\partial z}\cdot D + C_{NP}\right]. \quad (3)$$

The first term of Eq. (3) represents the change in the tip-substrate capacitance as the tip rises above the NP position. Indeed, as the NP shows up as a bump of height $D \simeq 10$ nm

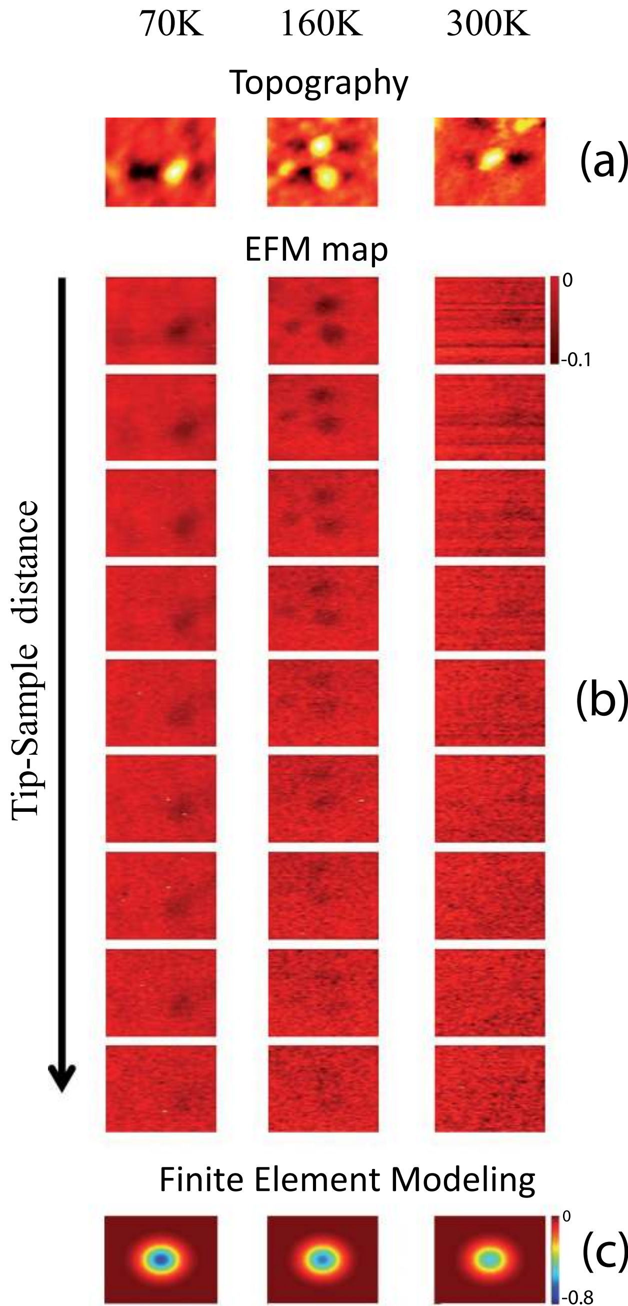

FIG. 3. Panels (a): Topography images of magnetite NPs taken at different temperatures. The full size width of the images are, respectively, W 180 nm, 270 nm, and 570 nm, from left to right. Panel (b): First harmonic of EFM signal, where each image column is acquired at T 70 K, 160 K, and 300 K, respectively. Note that the NP chosen for 3D maps presented typical size and capacitive signal with respect to other NP seen in large scans. Panel (c): Finite element simulation of the EFM signal for NPs with dielectric coefficient ϵ 1 and screening length λ $10D, D, 0$, respectively.

in the topography scan, when the tip is re-scanned with a constant offset h_j, it will also rise by the amount $D \simeq 10$ nm at the vertical of the NP position. Thus, it is important to notice that even a NP with no charge response, i.e., $\epsilon = 1$ and $\kappa = 0$, will be visible in the EFM image because of this first term, which is only related to the z-dependence of C_{sub} and does not include the charge response of the NP. This mechanism of EFM image forming was checked by finite element modeling[16] where we calculated C'' images, shown Fig. 3(c), for semiconducting NP of increasing carrier concentration, i.e., increasing charge compressibility. In this simulation, we

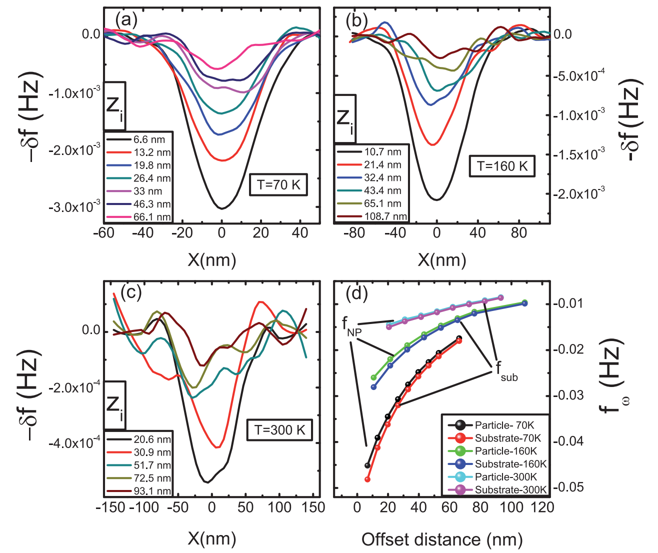

FIG. 4. Panels (a) (c): Frequency shift profile $\delta f(X)$ $(f_\omega(X)$ $f_{sub})$ extracted from the images shown Fig. 3, taken at different height offset h_j and different temperatures. The minimum in the curves correspond to the location of the NP. Panel (d): Frequency shift f_{sub} is $f_\omega(X)$ when measured far from the NP, and f_{NP} when measured at the vertical of the NP.

find that the NP with the smaller charge compressibility produces the largest change in the EFM image. Furthermore, as the charge compressibility increases, f_ω decreases due to a positive capacitive contribution that comes from the NP. This contribution C_{NP} is the second term in Eq. (3).

Using the fact that the frequency shift is proportional to the second derivative of the capacitance ($f \propto C''$) and that $C \propto z^\alpha$, Eq. (3) can be written as[16]

$$\frac{C_{NP}}{C_{sub}} = \frac{\alpha}{(\alpha - 2)}\frac{1}{f_{sub}}[\delta f - \delta f_{lift}], \tag{4}$$

where $\delta f = f_{NP} - f_{sub}$ and δf_{lift} represents the small change in the frequency of the tuning fork due to the substrate when the tip lifts while passing above the NP. All quantities on right hand side of Eq. (4) can be extracted from the 3D EFM map: δf_{lift} can be obtained from Fig. 4(d), δf can be obtained from the EFM profiles, Figs. 4(a) 4(c) (plotted in Fig. 5(a) as a function of offset height), and D can be obtained from the topographic image. The ratio $\frac{C_{NP}}{C_{sub}}$ obtained is shown Fig. 5(b)

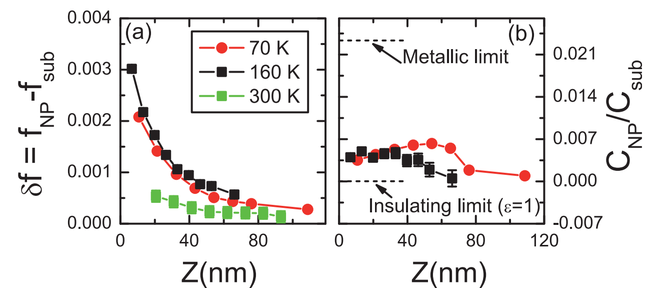

FIG. 5. Panel (a): Frequency shift difference δf obtained from the profile shown Fig. 4, taken at different height offset h_j and different temperatures. Panel (b): Contribution C_{NP}/C_{sub} of the NP to the capacitive signal at 160 K and 70 K, showing that the NP contributes to 0.3% of the full capacitive signal between the tip and the substrate. This NP contribution goes to zero at large tip sample distance and does not change with temperature, as expected for an insulating dielectric NP. The metallic and insulating limits are shown as dotted lines at low tip/sample distance for comparison.

as a function of the tip height offset for the two lowest temperatures. We find that this ratio goes to zero at large distance, as expected, because the NP contribution decreases as the height offset increases monotonically. This observation confirms the relevance of our analysis. As the height offset decreases, we find that the NP contribution to the total capacitance increases, reaching a maximum of 0.5%, for the two temperatures $T = 70\,\mathrm{K}$ and $T = 160\,\mathrm{K}$ (300 K data could not be analyzed due to poor signal/noise ratio seen in the Fig. 3). Within the experimental uncertainty, this shows that the charge response of the NP does not change with temperature. If the NPs were metallic, we would see a large change between the two temperatures as the Verwey temperature is between these two temperatures. This implies that the NP is insulating and that the main response of the NP to the electric field is through a dielectric response with $\epsilon > 1$. This conclusion was corroborated by XPS spectra of the NPs prepared under the same conditions that have shown that the NP was probably of the Fe_2O_3 stoichiometry, Fig. S3.

Before concluding, a few comments are in order. First, if the NP had no charge response ($\kappa = 0, \epsilon = 1$), the ratio C_{NP}/C_{sub} would remain equal to zero even close to the NP. In that case, scanning the NP in the X direction or lifting the tip of an height D, far from the NP, provides an equal change in f_ω, which cancel each other in the formula Eq. (4). This behavior was confirmed by finite element simulations, Fig. S2. In contrast, in the case of a finite dielectric response ($\epsilon > 1$) or a non-zero charge compressibility ($\kappa > 0$), C_{NP}/C_{sub} will deviate from zero as h_j decreases. Second, if the NP is perfectly metallic, the second term is null and C_{NP}/C_{sub} reaches the maximum value of 1.3%, shown Fig. 5(b), due to the fist term of Eq. (4). As a last comment, in this work, we only express the NP contribution relative to tip-substrate capacitance. However, using calibrated tip, whose capacitance to a flat sample is known, an absolute measure of C_{NP} could be obtained.

To conclude, we have shown that by acquiring 3D EFM maps of a single NP, it is possible to extract the tip-NP contribution to the capacitive EFM signal by substracting the tip-substrate capacitive contribution, which is known from the z dependence of the EFM signal. Applying the technique to undecanoic coated FeO_x NPs, we could establish that the NPs behave as insulating dielectric materials.

We acknowledge support from ANR Grant No. 10-0409-01 "QUANTICON" and ANR Grant No. 09-BLAN-0388-01 "CAMELEON." We acknowledge Philippe Marcus and Sandrine Zanna for XPS measurements.

[1]W. Lu, D. Wang, and L. Chen, Nano Lett. **7**, 2729 2733 (2007).
[2]W. Lu, Y. Xiong, A. Hassanien, W. Zhao, M. Zheng, and L. Chen, Nano Lett. **9**, 1668 1672 (2009).
[3]T. Mélin, H. Diesinger, D. Deresmes, and D. Stiévenard, Phys. Rev. B **69**, 035321 (2004).
[4]T. Mélin, H. Diesinger, D. Deresmes, and D. Stiévenard, Phys. Rev. Lett. **92**, 166101 (2004).
[5]M. Paillet, P. Poncharal, and A. Zahab, Phys. Rev. Lett. **94**, 186801 (2005).
[6]L. Fumagalli, D. Esteban Ferrer, A. Cuervo, J. L. Carrascosa, and G. Gomila, Nature Mater. **11**, 808 816 (2012).
[7]S. C. Dultz and H. W. Jiang, Phys. Rev. Lett. **84**, 4689 4692 (2000).
[8]L. Li, C. Richter, S. Paetel, T. Kopp, J. Mannhart, and R. C. Ashoori, Science **332**, 825 828 (2011).
[9]B. Wu, A. Zimmers, H. Aubin, R. Ghosh, Y. Liu, and R. Lopez, Phys. Rev. B **84**, 241410(R) (2011).
[10]S. Watanabe and M. Imada, J. Phys. Soc. Jpn. **73**, 3341 3350 (2004).
[11]E. J. W. Verwey, Nature **144**, 327 328 (1939).
[12]X. W. Li, A. Gupta, G. Xiao, and G. Q. Gong, J. Appl. Phys. **83**, 7049 (1998).
[13]A. V. Ramos, J. B. Moussy, M. J. Guittet, A. M. Bataille, M. Gautier Soyer, M. Viret, C. Gatel, P. Bayle Guillemaud, and E. Snoeck, J. Appl. Phys. **100**, 103902 (2006).
[14]N. Pinna, S. Grancharov, P. Beato, P. Bonville, M. Antonietti, and M. Niederberger, Chem. Mater. **17**, 3044 3049 (2005).
[15]F. F. J. Giessibl, Rev. Mod. Phys. **75**, 949 983 (2003).
[16]See supplementary material at http://dx.doi.org/10.1063/1.4790587 for the finite elements simulation details and the derivation of Eq. (4).